THE JOURNAL OF PHYSICAL CHEMISTRY B

Article

pubs.acs.org/JPCB

# The Hydrogen Catalyst Cobaloxime: A Multifrequency EPR and DFT Study of Cobaloxime's Electronic Structure

Jens Niklas,*[,†] Kristy L. Mardis,[‡] Rakhim R. Rakhimov,[§] Karen L. Mulfort,[†] David M. Tiede,[†] and Oleg G. Poluektov*[,†]

[†]Division of Chemical Sciences and Engineering, Argonne National Laboratory, Argonne, Illinois 60439, United States

[‡]Department of Chemistry and Physics, Chicago State University, Chicago, Illinois 60628, United States

[§]Center for Materials Research, Norfolk State University, Norfolk, Virginia 23504, United States

Supporting Information

**ABSTRACT:** Solar fuels research aims to mimic photosynthesis and devise integrated systems that can capture, convert, and store solar energy in the form of high-energy molecular bonds. Molecular hydrogen is generally considered an ideal solar fuel because its combustion is essentially pollution-free. Cobaloximes rank among the most promising earth-abundant catalysts for the reduction of protons to molecular hydrogen. We have used multifrequency EPR spectroscopy at X-band, Q-band, and D-band combined with DFT calculations to reveal electronic structure and establish correlations among the structure, surroundings, and catalytic activity of these complexes. To assess the strength and nature of ligand cobalt interactions, the $BF_2$-capped cobaloxime, $Co(dmgBF_2)_2$, was studied in a variety of different solvents with a range of polarities and stoichiometric amounts of potential ligands to the cobalt ion. This allows the differentiation of labile and strongly coordinating axial ligands for the Co(II) complex. Labile, or weakly coordinating, ligands such as methanol result in larger *g*-tensor anisotropy than strongly coordinating ligands such as pyridine. In addition, a coordination number effect is seen for the strongly coordinating ligands with both singly ligated $LCo(dmgBF_2)_2$ and doubly ligated $L_2Co(dmgBF_2)_2$ . The presence of two strongly coordinating axial ligands leads to the smallest *g*-tensor anisotropy. The relevance of the strength of the axial ligand(s) to the catalytic efficiency of $Co(dmgBF_2)_2$ is discussed. Finally, the influence of molecular oxygen and formation of Co(III) superoxide radicals $LCo(dmgBF_2)_2O_2^{\bullet}$ is studied. The experimental results are compared with a comprehensive set of DFT calculations on $Co(dmgBF_2)_2$ model systems with various axial ligands. Comparison with experimental values for the "key" magnetic parameters such as *g*-tensor and $^{59}Co$ hyperfine coupling tensor allows the determination of the conformation of the axially ligated $Co(dmgBF_2)_2$ complexes. The data presented here are vital for understanding the influence of solvent and ligand coordination on the catalytic efficiency of cobaloximes.

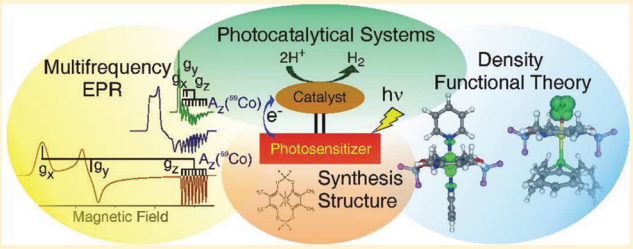


## INTRODUCTION

The production of carbon-neutral and sustainable fuel sources by solar energy conversion is considered to be a vital component of our future energy landscape.[1,2] Biology provides several examples for processes necessary to transform abundant solar energy to energy stored in the form of chemical bonds in small, energy-dense molecules, such as molecular hydrogen. Molecular hydrogen is generally considered as an ideal energy carrier, since its combustion is essentially pollution-free. A major goal in the field of solar $H_2$ production is to generate molecular systems that ideally have both a high turnover number (stability of the molecular device) and high turnover frequencies (efficiency of catalyst) using earth-abundant first-row transition metals rather than unsustainable precious metals. A variety of different catalysts designed toward this goal have been structurally and mechanistically characterized for the reduction of protons to molecular hydrogen (reviewed in[2,3]); however, both the efficiency and stability of these devices still need significant improvement.

The development of an efficient system for hydrogen generation driven by sunlight has even been termed a "Holy Grail" of solar-driven water splitting.[3] Among currently known complexes, cobaloxime compounds (cobalt macrocycles with diglyoxime ligands) have been emerging as productive electrocatalysts for the reaction $2H^+ + 2e^- \rightarrow H_2$ with low overpotential in the presence of a proton source in organic solvents. Cobaloximes are not only among the best synthetic transition metal complexes known for $H_2$ production but also relatively easy to synthesize, oxygen-tolerant, are amenable for coupling to natural and artificial photosynthetic systems,[3,4] and rely only on earth-abundant materials. The pseudomacrocyclic cobaloxime compounds were originally developed and investigated as vitamin-$B_{12}$ analogs[5,6] and have been extensively studied as a model system for vitamin $B_{12}$.[7−9] About 20 years

**Received:** September 28, 2011
**Revised:** January 6, 2012
**Published:** February 29, 2012

ACS Publications © 2012 American Chemical Society

later, Connolly and Espenson found that difluoroborylcobaloxime $Co(dmgBF_2)_2$ catalyzes proton reduction in acidic media.[10]

The urgent need for earth-abundant materials capable of solar energy conversion has prompted renewed interest in the catalytic properties of cobaloxime compounds. Both electrocatalytical systems for hydrogen evolution that utitilize cobaloxime and systems using photosensitizers have been reported.[3,11−18] Recently, the first photocatalytic supramolecular assemblies based on pyridyl coordination of a variety of photosensitizers to the Co(II) center of the cobaloxime macrocycle have been described.[4,19−22] However, a significant problem for many cobaloxime compounds is their low stability at low pHs and rapid decomposition, which limits their general utility for hydrogen catalysis, while the ($BF_2$-capped) difluoroborylcobaloximes, such as $Co(dmgBF_2)_2$ (Figure 1),

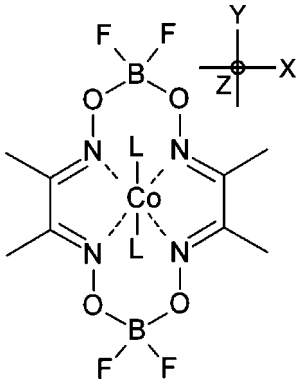


**Figure 1.** Molecular structure of the $BF_2$-capped cobaloxime $Co(dmgBF_2)_2$ investigated in this work. The molecular axes system is also depicted. The *g*-tensor principal axes and the principal axes of the $^{59}Co$ hyperfine coupling tensor (*A*-tensor) are expected to be collinear to the molecular axes system unless molecular oxygen is bound.

have been found to be more resistant toward acidic hydrolysis than H-capped cobaloxime compounds.[3,10,23] In addition, the reduced nucleophilicity of its hydride derivative limits undesired hydrogenation reactions. Furthermore, for the $BF_2$-capped cobaloxime, the ground state is more easily reduced with its Co(II)/Co(I) potential about 0.5 V more positive than the H-capped cobaloxime.[3] Another benefit is that the presence of a conjugated bridging ligand facilitates the transfer of electrons to the cobalt ion. The $BF_2$-capped cobaloxime $Co(dmgBF_2)_2$ studied here is quite resistant to oxidation by molecular oxygen and the ensuing degradation of the cobalt macrocycle. These factors make it a better model system for studying the interaction of the cobalt complex with molecular oxygen, as compared with H-capped cobaloxime.[24]

The catalytic efficiency is determined to a large extent by the electronic structure of the cobaloxime. The electronic structure, in turn, is strongly influenced by the macrocycle's surroundings and, in particular, by the ligand(s) directly bound to the central metal ion. In addition, other secondary interactions, such as hydrogen bonding to the fluorine atoms and the dielectric properties of the medium, cannot be neglected. An excellent illustration of the importance of the surroundings is the redox potential. The cobaloxime Co(II)/(I) reduction potential is sensitive to its coordination environment and shifts significantly on pyridyl coordination to the Co(II) center.[3,4,21] Thus, the knowledge of the electronic properties is essential for an understanding of the catalytic properties of the complex.

So far, only cursory experimental data regarding changes in the electronic structure as a result of axial coordination are available. The resting state of cobaloxime's catalytic cycle is $3d^7$ low spin Co(II).[25] Since the highest occupied molecular orbital of the Co(II) complex, which carries a single unpaired electron, has mainly $d_{z2}$ character, the effect of axial coordination by fifth and sixth ligands to the cobalt ion is crucial for the function of cobaloxime, particularly in catalytic processes involving axial ligand exchange. Electron paramagnetic resonance (EPR) spectroscopy is an excellent tool to characterize any changes in electronic structure that result from changes to the surrounding environment or properties of the orbital carrying the unpaired electron. Changes in the electronic properties can then be correlated with different catalytic efficiencies of cobaloxime.

Several EPR studies on cobaloxime compounds exist, but there are a number of inconsistencies and gaps in the published data, for example, refs 24−35. First, almost all studies focus on H-capped cobaloxime, and to the best of our knowledge, there has been only one previous cursory EPR study of $Co(dmgBF_2)_2$.[25] The second drawback is that most previous cobaloxime EPR studies (including the one by Bakac and coworkers on $Co(dmgBF_2)_2$) performed EPR spectroscopy only at the conventional X-band frequency (9−10 GHz). In most cases, the X-band spectra are very congested, with *g*-tensor anisotropy and $^{59}Co$ hyperfine interaction having the same order of magnitude, which makes it difficult to determine the principal components of the *g*-tensor, leaving one of the most important parameters far from precisely determined. In fact, in many studies, both the *g*-tensor and the $^{59}Co$ *A*-tensor were reported as axial, whereas it is shown in our study that in nearly all cases, both tensors are essentially rhombic. Furthermore, the previous studies were either lacking quantum mechanical calculations completely or the treatment was restricted to Hückel theory.

Here, we use EPR spectroscopy at X-band (9 GHz), Q-band (34 GHz), and D-band (130 GHz) microwave frequencies to distinguish clearly among field-dependent and field-independent parameters. The multifrequency approach allows us to determine *g*-tensor anisotropy and hyperfine splitting due to the central metal ($^{59}Co$) and coordinating solvents molecules/ligands (L) that have $^{14}N$, $^{15}N$, or $^{31}P$ magnetic nuclei. A variety of different solvents from different groups are studied, including (i) polar protic solvents, (ii) polar aprotic solvents, (iii) nonpolar solvents, and with and without potential ligands to the central cobalt ion. The experimental investigation was accompanied by an extensive density functional theory (DFT) study on the cobaloxime, taking into account a variety of different possible conformations of the cobaloxime macrocycle and ligand/solvent molecules.

The catalytically relevant ligands studied both in experiment and calculation include the "small and simple" ligand pyridine as well as two rather bulky organic molecules, *N*-cyclohexyl-*N*′-4-pyridyl-1,7-dipyrrolidinylperylene-3,4:9,10-tetracarboxylic acid bisimide (PDI) and triphenylphosphane ($PPh_3$) (Figure S1 of the Supporting Information). The PDI scaffold is widely used in many light-harvesting applications because of its high extinction coefficient, broad absorbance and redox tunability, and exceptional structural integrity and thus presents an attractive alternative to other photosensitizers that contain precious metals. PDI derivatives are most often employed as acceptor fragments in donor-bridge-acceptor constructs.[36] A supramolecular cobaloxime assembly was recently reported

with a pyridyl-functionalized PDI molecule coordinated to cobaloxime, acting as a photosensitizer.[21]

Triphenylphosphine ($PPh_3$) is the second bulky ligand studied. The central phosphorus atom acts as the ligating atom of $PPh_3$, where the $^{31}P$ nuclear spin of $I = 1/2$ allows the hyperfine interaction of the phosphorus atom with the unpaired electron to be monitored. Interaction of cobaloximes with molecular oxygen was studied on an example of an $O_2$:Co:$PPh_3$ complex that efficiently formed a stable but reversible paramagnetic adduct. The oxygenation is found to dramatically change the EPR spectrum of cobaloxime, resulting in a pronounced reduction of *g*-tensor anisotropy and decrease in both $^{31}P$ and $^{59}Co$ hyperfine interaction, which is consistent with a pronounced shift of electron spin density to molecular oxygen. We anticipate that this comprehensive study of the changes in the electronic properties in response to a variety of environmental factors can be correlated with demonstrated catalytic efficiencies of cobaloxime and eventually provide a predictive tool for the design of new cobaloxime catalyst structures.

## EXPERIMENTAL PROCEDURES

**Sample Preparation.** All commercial reagents, including organic solvents, were of ACS grade and purchased from Sigma-Aldrich unless otherwise noted. $^1H$ NMR (500 MHz) was performed on a Bruker DMX 500 spectrometer and referenced to TMS or a residual solvent peak as an internal standard. ESI-MS was conducted on a ThermoFisher LCQ Fleet from dilute acetonitrile or methanol solutions. UV-vis absorbance measurements were performed on a Shimadzu UV-1601 spectrophotometer. The synthesis of the cobaloxime $Co(dmgBF_2)_2{\cdot}H_2O$ was carried out as previously described and matched all characterization methods.[23] Solvents were methanol, glycerol/$H_2O$, acetone, toluene, dichloromethane ($CH_2Cl_2$), and dimethylformamide (DMF). The synthesis of *N*-cyclohexyl-*N*′-4-pyridyl-1,7-dipyrrolidinylperylene-3,4:9,10-tetracarboxylic acid bisimide (PDI) was described previously.[21] $^{15}N$-labeled pyridine was obtained from Cambridge Isotope Laboratories (Andover, MA). $Co(dmgBF_2)_2{\cdot}H_2O$ was dissolved in the respective solvent (or solvent mixture, possibly containing potential ligand molecules) to yield a 1−3 mM solution. The solutions were thoroughly purged with $N_2$ before filling the quartz tubes used for the EPR measurements under nitrogen atmosphere in a drybox. The samples were then frozen quickly in liquid nitrogen. The samples of the oxygen adduct $LCo(dmgBF_2)_2O_2$, were prepared outside the drybox under aerobic conditions and frozen quickly in liquid nitrogen.

**EPR Spectroscopy.** CW X-band (9 GHz) EPR experiments were carried out with a Bruker ELEXSYS E580 EPR spectrometer (Bruker Biospin, Rheinstetten, Germany), equipped with a $TE_{102}$ rectangular EPR resonator (Bruker ER 4102st) and a helium gas-flow cryostat (Air Product, Allentown, PA). The temperature was controlled by a Lakeshore cryogenic temperature controller (Westerville, OH).

Pulse X-band experiments were performed on the same spectrometer, using a Flexline dielectric ring resonator (Bruker ER 4118X-MD5 or Bruker EN 4118X-MD4-W1) and a helium gas-flow cryostat (CF935, Oxford Instruments, UK). The temperature was controlled by an ITC (Oxford Instruments, UK).

CW Q-band (34 GHz) EPR experiments were carried out with the same EPR spectrometer equipped with a Q-band bridge (Bruker ER 051 QG), a cylindrical EPR resonator (Bruker ER 5106 QT-W), and a helium gas-flow cryostat (CF935, Oxford Instruments). The temperature was controlled by an ITC (Oxford Instruments, UK). The microwave frequency was monitored by a frequency counter (5352B, Hewlett-Packard).

High-frequency EPR measurements were performed on a home-built D-band (130 GHz) spectrometer equipped with a single-mode $TE_{011}$ cylindrical cavity.[37] EPR spectra of the samples were recorded in pulse mode to remove the microwave phase distortion due to fast-passage effects. The absorption line shape of the EPR spectra was recorded by monitoring the electron spin echo (ESE) intensity from a two-microwave-pulse sequence as a function of the magnetic field. The duration of a $\pi/2$ microwave pulse was 40−60 ns, and typical separation times between microwave pulses were 150−300 ns. All D-band spectra have been pseudomodulated to facilitate comparison with the respective X- and Q-band spectra.[38]

Data processing was done using Xepr (Bruker BioSpin, Rheinstetten) and the Matlab 6.5 (MathWorks) environment. The magnetic parameters were obtained from theoretical simulation of the EPR and ENDOR spectra. The simulations were performed using the EasySpin software package (version 3.1.7).[39] Quadrupole interactions were not included, since within the first order of perturbation theory, they do not contribute to the EPR spectra. Several simulations were repeated with the program SimFonia, version 1.25 (Bruker BioSpin, Rheinstetten, 1996), using second-order perturbation theory, and delivered virtually identical parameters. The accuracy in determination of the electronic *g*-tensor for the set of multifrequency EPR spectra is estimated to be ±0.001.

**Density Functional Theory Calculations.** Starting structures for all geometry optimizations presented in this paper were obtained from the coordinates of the crystal structure of $Co(dmgBF_2)_2$ with acetonitrile as axial ligands, provided in the Supporting Information. This structure is very similar to the one described by Bakac et al. for $L_2Co(dmgBF_2)_2$ with methanol as axial ligand. The geometry optimizations were carried out using DFT with the B3LYP functional[40−42] using the 6-31G* basis set as implemented in PQSMol.[43] All structures were first optimized in the gas phase, and the resulting structures were reoptimized with solvent effects included by employing the continuum solvation model COSMO with a dielectric constant set to 80.[44] Geometry optimizations were also performed with lower dielectric constants and led to nearly identical structures.

In addition, a selected set of geometry optimizations were performed using larger basis sets with the program package ORCA.[45] These geometry optimizations again led to nearly identical structures and, subsequently, *g*-values. After confirming by the absence of imaginary frequencies that the stationary points obtained were minima, the spectroscopic parameters were obtained via single point DFT calculations, performed with the program package ORCA.[45] For all calculations of magnetic parameters, the program ORCA with the B3LYP functional was used in combination with the TZVP triple-$\zeta$ basis set of Ahlrichs and co-workers on all atoms except cobalt.[46,47]

For the transition metal $^{59}Co$, the Wachters basis set was used.[48,49] The Wachters basis set has proven quite successful for transition-metal compounds and is well suited for the description of structures, energies, and other properties (see e.g, refs 50 and 51). These single-point calculations also employed COSMO to account for the dielectric screening of


dx.doi.org/10.1021/jp209395n | J. Phys. Chem. B 2012, 116, 2943−2957

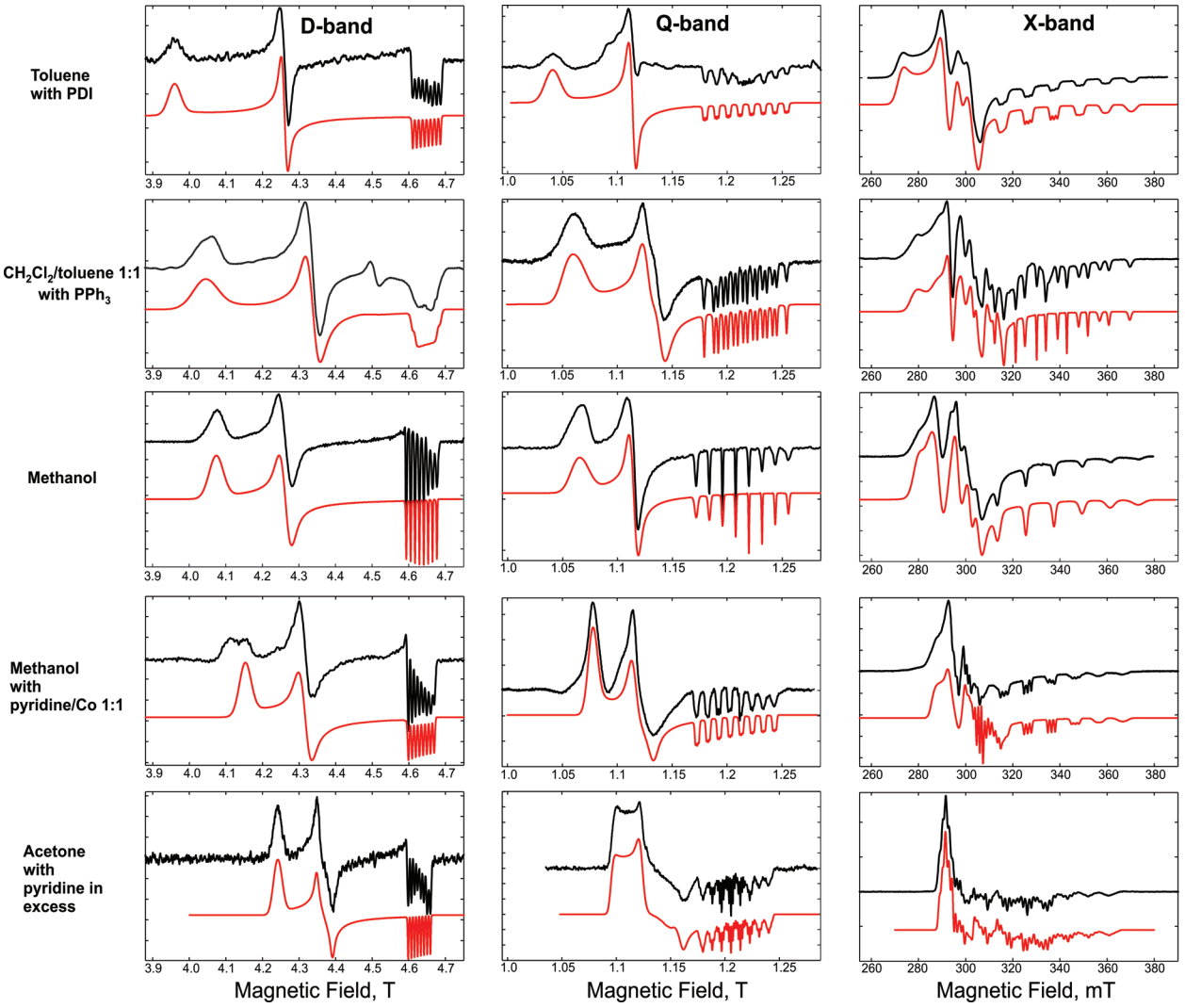


**Figure 2.** EPR spectra of the cobaloxime $Co(dmgBF_2)_2$ in different solvents recorded at different microwave frequencies (D-band, Q-band, X-band) at cryogenic temperatures. The field-swept ESE-detected D-band spectra have been pseudomodulated. Q-band and X-band spectra are CW EPR spectra. From the spectrum of cobaloxime in methanol with pyridine/Co in a 1:1 ratio, a minor contribution of the nonpyridine coordinated species has been subtracted. Simulations are depicted in red. Figure S2 (Supporting Information) provides these D-band spectra and additional D-band spectra without pseudomodulation.

surrounding molecules. The principal *g*-values were calculated employing the coupled-perturbed Kohn-Sham equations[52] in conjunction with a parametrized one-electron spin-orbit operator. The magnetic dipole and the isotropic Fermi contact contributions to the hyperfine coupling were calculated for all atoms, and for $^{59}Co$, second-order spin-orbit hyperfine contributions were also calculated.

In an additional set of calculations, the effect of the displacement of the central cobalt ion from the plane was systematically investigated. The complex contained a single pyridine molecule as the axial ligand in the "boat towards pyridine" conformation. A restricted geometry optimization was performed with the cobalt ion being pushed/pulled systematically in and out of the plane of the macrocycle using a torsion constraint (Co−N−N−N, Figure 1). The planar nature of the macrocycle portion of the complex was maintained by constraining the nitrogen atoms to remain in-plane via constraining the torsion angle of the four nitrogen atoms to the initial, unconstrained value of −0.0158°. The spectroscopic parameters were obtained via single point DFT calculations as described above.

## RESULTS AND DISCUSSION

**Experimental Results - EPR under Anaerobic Conditions.** Figure 2 shows selected EPR spectra of the cobaloxime $Co(dmgBF_2)_2$ in several different solvents or solvent mixtures under anaerobic conditions, recorded at X-band (9−10 GHz), Q-band (34 GHz), and D-band (130 GHz) microwave frequencies. The multifrequency approach allows us to clearly distinguish among magnetic field-dependent parameters (electronic *g*-tensor) and magnetic field-independent parameters (hyperfine coupling tensors, *A*-tensors).

We will first discuss the D-band spectra, since their analysis is clearest. At D-band, the *g*-tensor anisotropy of $Co(dmgBF_2)_2$ is by far larger than the other magnetic interactions, that is, any hyperfine interaction, and the line width. All our frozen solution D-band EPR spectra show a substantial *g*-tensor anisotropy ($g_x - g_z > 0.18$) and are typical for a low-spin $d^7$ ($S = 1/2$) electronic configuration of $^{59}Co$. This is in complete agreement


dx.doi.org/10.1021/jp209395n | J. Phys. Chem. B 2012, 116, 2943−2957

Table 1. EPR Simulation Parameters for the Cobaloxime $Co(dmgBF_2)_2$ in Different Solvents[a]

| solvent, ligand(s) | $g_x$[b] | $g_y$[b] | $g_z$[b] | \|A\| ($^{59}$Co), MHz | \|A\| ($^{14}$N), MHz | \|A\| ($^{31}$P), MHz |
|---|---|---|---|---|---|---|
| glycerol/$H_2O$ 60:40 (v/v) | 2.2750 | 2.1785 | 2.0065 | 15, 15, 329[c] | n/a | n/a |
| methanol | 2.2840 | 2.1820 | 2.0080 | 53, 20, 338[c] | n/a | n/a |
| dimethylformamide (DMF) | 2.2600 | 2.1695 | 2.0077 | 60, 50, 302[c] | n/a | n/a |
| toluene, PDI/Co 1:1 | 2.3473 | 2.1815 | 2.0000 | 85, 10, 306[c] | 30, 30, 40 | n/a |
| methanol pyridine/Co 1:1 | 2.2380 2.2610 | 2.1530 | 2.0058 | 10, 10, 285[c] | 33, 36, 43 | n/a |
| methanol pyridine/Co 10:1 | 2.1910 | 2.1270 | 2.0080 | 105, 148, 242 | 36, 39, 48 | n/a |
| acetone/pyridine 1:1 (v/v) | 2.1895 | 2.1278 | 2.0077 | 110, 148, 243 | 36, 39, 48 | n/a |
| $CH_2Cl_2$/toluene 1:1 (v/v) with $PPh_3$ | 2.3000 | 2.1425 | 1.9995 | 36, 10, 249[c] | n/a | 300, 300, 358 |
| $CH_2Cl_2$/toluene 1:1 (v/v) with $PPh_3$ and $O_2$ | 2.0390 | 2.0014 | 1.9879 | 28[c], 32, 13 | n/a | 20, 37, 37 |

[a]The same set of parameters was used to simulate X-band, Q-band, and D-band spectra. Note that the signs of the hyperfine coupling constants $A_x$, $A_y$, and $A_z$ could not be determined by analysis of the EPR spectra. Thus, only the magnitude is given. The $^{14}$N hyperfine coupling constants refer to the axial ligands, not to the macrocycle (equatorial) nitrogen atoms. [b]The accuracy in determination of the electronic $g$-tensor for the set of multifrequency EPR spectra is estimated to be ±0.001. [c]In these cases, the hyperfine coupling constants $A_x$ and $A_y$ were estimated from the line width, while for the superoxide only $A_x$ was estimated from the linewidth.

with previous investigations of several cobaloximes and related compounds.[25,30,33,53] Hence, the (pseudomodulated) D-band spectra allow a straightforward determination of the three principal values of the electronic $g$-tensor, which was found in all cases to be rhombic.

In contrast, many previous studies of cobaloxime at lower magnetic fields approximated the $g$-tensor to be axial. The values obtained from analysis of the D-band spectra were used as constraints in the simulation of X-band and Q-band data. In the following, we will refer to the principal $g$-values as $g_x$ (for $g_{max}$), $g_y$ (for $g_{mid}$), and $g_z$ (for $g_{min}$). In all cases, the smallest principal $g$-value $g_z$ is found to be close to the value of a free electron ($g_e$). This result is expected for a complex in which the unpaired electron resides preferentially on the $d_{z2}$ orbital (see below for a more detailed discussion). The largest $g$-tensor anisotropy ($g_x - g_z > 0.34$) is found in the case of a 1:1 ratio of PDI/Co (see Table 1).

The presence of PDI in the toluene solution could result in a mixture of doubly ligated, singly ligated, and nonligated cobaloxime complexes, depending on the free enthalpy of the respective complexes. Since $Co(dmgBF_2)_2$ is minimally soluble in neat toluene, at least one PDI molecule must be ligated to a cobaloxime in solution. The spectrum shows no indication of the presence of several paramagnetic species, demonstrating that only cobaloxime with one axial ligand is present. This conclusion is clearly verified by analysis of the ligand superhyperfine structure ($^{14}$N) at lower magnetic fields (see below). The presence of triphenylphosphane ($PPh_3$) in a solution of $CH_2Cl_2$/toluene (1:1) results in a slightly lower $g_x$ value than observed for PDI in toluene. This value is similar to that in methanol and several other neat solvents without strong axial ligand, which have $g_x$ values around 2.26−2.28 (see Table 1 and Figure S2 of the Supporting Information). Interestingly, the $g_y$ value is much smaller than in these other solvents, a property that has been also detected for H-capped cobaloxime.[29,33] The unusual ratio of $g_x/g_y$ has been explained as a $PPh_3$-induced distortion of the macrocycle.[29] The possible $PPh_3$-induced distortion of the macrocycle is discussed below in more detail.

Smaller $g$-tensor anisotropy is found when pyridine is present in slight stoichiometric excess as compared with the cobaloxime. The smallest $g$-tensor anisotropy ($g_x - g_z \approx 0.18$) is found in the case of a large pyridine excess with respect to the cobaloxime. The spectrum shows no sign of the presence of multiple species, indicating that two pyridine molecules act as axial ligands. In all D-band spectra, the hyperfine structure of $^{59}$Co ($I = 7/2$) is resolved only at $g_z$ orientation (high-field edge,) resulting in a splitting into $2I + 1 = 8$ lines. In the case of $PPh_3$ as axial ligand, the $^{59}$Co hyperfine structure is not resolved, even at the high-field edge. This is due to the substantial $^{31}$P hyperfine interaction in addition to the $^{59}$Co hyperfine interaction (see Table 1 and discussion below).

At Q-band frequency, the $g$-tensor anisotropy is resolved in most cases, whereas at X-band frequency, the $g$-tensor anisotropy is generally unresolved, since the cobalt hyperfine interaction is of comparable magnitude. As in the D-band spectra, the cobalt hyperfine structure is resolved only for $g_z$, but for the $A_x$ and $A_y$ components of the $^{59}$Co $A$-tensor, only an upper limit can in most cases be estimated by line broadening. The accuracy of determination of $A_x$ and $A_y$ is thus lower than for $A_z$. To determine $A_x$ and $A_y$ more precisely, we performed pulsed ENDOR and pulsed ELDOR-detected NMR experiments at X-band frequency on cobaloxime in methanol. Unfortunately, we were not able to detect signals of $^{59}$Co in ELDOR-detected NMR experiments. Only weak and broad ENDOR signals were detected, which we attribute to $^{59}$Co (Figure S4 of the Supporting Information). The strongly anisotropic $^{59}$Co $A$-tensor and the non-negligible quadrupolar coupling are most probably responsible for this.

The chemical nature and number of axial ligands can in many cases not be determined by inspection of the EPR spectra. However, if the coordinating atom of the axial ligand molecule possesses a magnetic nucleus ($I \neq 0$), the hyperfine interaction with the unpaired electron of the cobalt ion can deliver the necessary information. For pyridine or PDI with their nitrogen ($I(^{14}N) = 1$) atom as ligand, a superhyperfine structure can be observed, at least in the high-field part, of the X-band and Q-band EPR spectra. For the samples with a stoichiometric ratio of PDI to $Co(dmgBF_2)_2$, each resolved cobalt hyperfine line is split into three lines with equal intensity (1:1:1) and demonstrates the presence of one nitrogen axially coordinating the Co(II) ion. The same superhyperfine structure is observed for 1:1 pyridine/Co, indicating that also here, only one nitrogen is axially coordinating the cobalt ion. In contrast, in the case of a large excess of pyridine, the superhyperfine structure observed consists of five lines with an intensity ratio of 1:2:3:2:1. This pattern is indicative for two magnetically equivalent nitrogen atoms that are interacting with the same paramagnetic cobalt


dx.doi.org/10.1021/jp209395n | J. Phys. Chem. B 2012, 116, 2943−2957

ion. A smaller excess of pyridine (<10:1) results in a mixture of doubly- and singly coordinated complexes. Similar results have been obtained for H-capped cobaloxime.[28,35]

To exclude the possibility that the strongly interacting nitrogen atoms(s) responsible for the superhyperfine structure are from the equatorial dimethylglyoxime ligands, we performed these measurements also with $^{15}$N-labeled ($I$ = 1/2) pyridine instead (Figure S3 of the Supporting Information). The superhyperfine structure changed with respect to the $^{14}$N-labeled pyridine, exhibiting a pattern of 1:1 for singly ligated cobaloxime and 1:2:1 for doubly ligated cobaloxime. This proves unequivocally that the resolved superhyperfine structure is due to the axial ligand(s). We did not observe in any case resolved hyperfine structure from the equatorial (macrocycle) nitrogen atoms, indicating that their hyperfine couplings are rather small, at least for $A_z$ (assuming that the $A$-tensor is close to collinear to the $g$-tensor). This is in agreement with previous studies of H-capped cobaloximes, in which also hyperfine coupling constants of the equatorial nitrogen atoms could not be determined from the EPR spectra.[29,32] The quantitative appearance of cobaloxime complexes singly ligated by PDI or pyridine in samples with a 1:1 stoichiometric ratio demonstrates the far higher affinity of the nitrogen-containing pyridine bases and derivatives to the central Co(II) ion as compared with the oxygen-containing polar (e.g., acetone) or polar and protic (e.g., methanol) solvents, which are readily replaced as axial ligands.

Somewhat different results were obtained for $PPh_3$ as axial ligand. In the case of the bulky ligand $PPh_3$, the same EPR spectrum was found for different stoichiometric ratios of cobalt and $PPh_3$, as long as the $PPh_3/Co(dmgBF_2)_2$ ratio was greater than 1 (Figure 2). This is a clear sign of the stability of the singly ligated complex, if compared with pyridine as the axial ligand, in which a 10-fold stoichiometric excess results mostly in doubly ligated cobaloxime complexes. Our observation is in agreement with previous results obtained in a study of H-capped cobaloxime,[26,29] in which no doubly ligated cobaloxime was observed when $PPh_3$ or related compounds were present. All these results indicate that the binding of a second $PPh_3$ molecule is not as thermodynamically favorable as it is for pyridine and that the singly ligated $PPh_3$:$Co(dmgBF_2)_2$ complex is rather stable. A possible reason for this behavior is that the binding of the first bulky ligand molecule results in a displacement of the cobalt ion from the equatorial plane of the macrocycle, possibly including a deformation of the macrocycle. This would make the binding of a second bulky ligand thermodynamically unfavorable and also lower the accessibility of the cobalt ion for catalytic reactions. Since the Co(II)-coordinating part of PDI is identical to pyridine, we consider the explanation that PDI directly causes a much more pronounced cobalt displacement or macrocycle distortion unlikely. A more detailed discussion is given below. In a study of H-capped cobaloxime, Baumgarten et al. observed a larger $g$-anisotropy when using a toluene/THF mixture instead of methanol.[33] For our $BF_2$-capped cobaloxime, the increase in the $g$-tensor anisotropy is even larger in neat toluene with PDI. It should be mentioned that the experimental data do show a large increase in $g_x$ as compared with pyridine, but the $^{59}$Co hyperfine interaction stays similar in magnitude. The effect of cobalt displacement from the plane is discussed in more detail in the DFT section, where we performed a systematic study of the dependence of magnetic parameters on the Co(II) out-of-plane distance.

**Correlation Dependence of *g*- and *A*-Tensors.** For simulation of the EPR spectra, it has been assumed that the $g$-tensor principal axes and the principal axes of the $^{59}$Co $A$-tensor are collinear. The ligand superhyperfine principal axes ($^{14}$N, $^{31}$P) were assumed to be collinear to the $g$-tensor principal axes, as well. A rotation of the $A$-tensor with respect to the $g$-tensor did not lead to an improved fit. The assumption that the $g$-tensor principal axes and the $^{59}$Co $A$-tensor principal axes are close to collinear is also justified on the basis of the theoretical DFT calculations (see below). A similar observation concerning the collinearity of the $g$-tensor and $^{59}$Co $A$-tensor has also been made for H-capped cobaloxime.[27,33]

Figure 3a shows a plot of the $g_y$ values vs $g_x$ values. Ignoring the large, bulky ligands PDI and $PPh_3$, there exists a linear

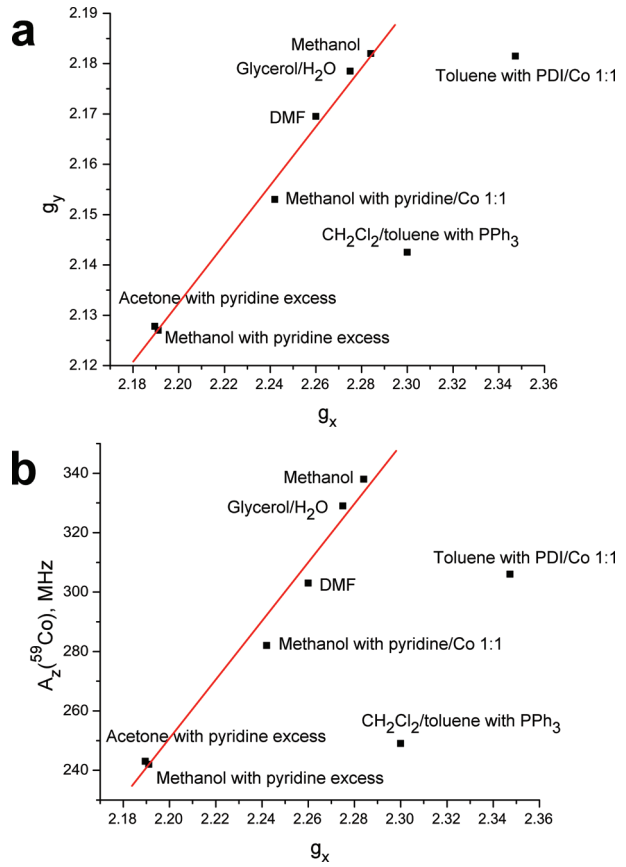


**Figure 3.** Plots of $g_y$ and $|A_z|$ ($^{59}$Co) vs $g_x$ for the cobaloxime $Co(dmgBF_2)_2$ in different solvents. All data are obtained from experiments.

relation between $g_y$ and $g_x$. A linear interpolation to smaller $g_x$ values intersects the point where both $g_x$ and $g_y$ are near the free electron $g$ value, $g_e$ ($g_x$, $g_y \sim g_e$). This linear dependence can be justified on the basis of the simplified Stone formula as a first approximation for the prediction of $g$-tensor anisotropy due to spin-orbit coupling,

$$\Delta g \sim (\rho \times \zeta)/\Delta E \quad (1)$$

where $\Delta g$ is the deviation from $g_e$; $\zeta$ is the spin-orbit coupling constant for the respective atom; $\rho$ is the unpaired spin density in the particular atomic orbital containing the unpaired electron; and $\Delta E$ is the energy difference between the orbital containing the unpaired electron and lower or higher laying orbitals.[54] According to Stone's theory of $g$ values, negative


dx.doi.org/10.1021/jp209395n | J. Phys. Chem. B 2012, 116, 2943−2957

deviation of $g$ values from the free electron value is due to spin-orbit coupling with empty higher-lying orbitals whereas spin-orbit coupling with lower-lying occupied orbitals leads to positive deviations.

The difference between $\Delta g_x$ and $\Delta g_y$ is related to the symmetry properties of the particular atomic orbitals. Total deviation of the $g$-values is a sum of the deviations induced by each atom in the molecule. Because Co(II) in the $3d^7$ configuration has the biggest spin-orbit coupling constant, 515 $cm^{-1}$, as compared with other atoms in the molecule,[55] the analysis can be simplified by taking into account only Co orbitals. Thus, if the electronic structure of the cobaloxime does not change substantially upon change of the axial ligand, that is, the molecular orbitals are in the first-order approximation the same combination of the atomic orbitals, the plot of $g_y$ vs $g_x$ should demonstrate linear dependence. As was shown previously,[53,56,57] the complete absence of axial ligands results in very large $g$-tensor anisotropy and very large $^{59}$Co hyperfine coupling constants, much larger than observed in our study. We thus conclude that we always have at least a weak axial ligation of the Co(II) ion. According to eq 1, the same linear behavior should hold for the plot of $A_z$ vs $g_x$ or $g_y$ because $A_z$ is proportional to the spin density of the unpaired electron within the first order of approximation. Indeed, the plot of $A_z$ vs $g_x$ (Figure 3b) shows also linear dependence. This is important, since the slopes of the lines in Figure 3 are sensitive characteristics of the electronic structure of the compound and might be a reference point for testing the validity of DFT calculations along with $g$- and $A$-tensors.

A large $g$-tensor anisotropy for $Co(dmgBF_2)_2$ is observed for "weakly" coordinating ligands such as alcohols, acetone, or DMF, in which an oxygen atom is involved in coordination of the cobalt ion. Ligands termed "weakly coordinating or labile" can be easily replaced by small amounts of another type of ligand referred to as "strongly coordinating". Two general types of "strong" Co(II) coordination can be distinguished. In the six-coordinated $L_2Co(dmgBF_2)_2$ complex, two strong axial ligands such as pyridine are bound to the central cobalt ion. In the five-coordinated $LCo(dmgBF_2)_2$, only one strong axial ligand is present. If in the latter case a second, weak ligand such as methanol or acetone binds at the open axial coordination site cannot be verified on the basis of our experimental results.

In both cases (singly or doubly ligated by pyridine) the $g$-tensor anisotropy is significantly smaller than for the weakly coordinating solvents such as methanol. The doubly ligated pyridine/cobaloxime complex exhibits even smaller $g$-tensor anisotropy than the singly ligated cobaloxime. Since cobaloxime in a solvent of "weak" ligand molecules has most probably two axial ligands, the $g$-tensor anisotropy is unlikely to be predominantly caused by displacement of the Co(II) ion from the equatorial plane. More likely, the interaction strength with ligand molecules leads to reduced $g$-tensor anisotropy. The relative small hyperfine interaction with the pyridine nitrogen atoms contradicts the assumption of a substantial shift of unpaired spin density from Co(II) to the ligand molecules, which is supported by the DFT calculations (see below). Concomitantly to the reduced $g$-tensor anisotropy, a reduction of the $^{59}$Co $A_z$ value is found, and both $A_x$ and $A_y$ increase in magnitude. The main effect of axial ligand field could be a modification of the $\Delta E$ term in eq 1 or a reduction of spin density in the $d_{z2}$ orbital (or both), which seems unlikely. A direct determination of relative orbital energies is complicated, since multiple parameters influence the relation between magnetic properties and orbital energies.[57]

So far, the two bulky ligands PDI and $PPh_3$, which do not fit into the rather simple model described above, have not been discussed. Unfortunately, because of the hydrophobic nature of these ligands, their complexes with cobaloxime can exist only in nonpolar solvents such as toluene or a $CH_2Cl_2$/toluene mixture. On the other hand, the hydrophilic nature of cobaloxime does not allow the existence of pyridine/cobaloxime complexes in strongly nonpolar solvents and thus prevents the direct comparison of magnetic resonance parameters with bulky hydrophobic ligands in the same solvents. These two bulky ligands, in combination with the nonpolar solvents, also exhibited different thermodynamic properties, showing a lower affinity for a second molecule to ligate the Co(II) ion. This matter will be further addressed in the DFT section.

**Experimental Results - EPR under Aerobic Conditions.** It is well-known that many Co(II) complexes, including cobaloximes, form adducts with molecular oxygen.[24,25,58−60] The $BF_2$-capped cobaloxime $Co(dmgBF_2)_2$ studied here is expected to be quite resistant against oxidation by molecular oxygen and subsequent degradation of the cobalt macrocycle.[3] This makes it the ideal cobaloxime for studying the interaction of the complex with molecular oxygen, as compared with previous studies of the H-capped cobaloxime. A certain resistance against oxidation and degradation by molecular oxygen is also desirable for any catalyst involved in hydrogen production.

Bakac and co-workers already observed the reversible binding of molecular oxygen by $Co(dmgBF_2)_2$ in a variety of different solvents, including water, methanol, acetonitrile, and acetone.[25] Schrauzer and Lee studied H-capped cobaloxime using different bases as axial ligands.[24] The EPR spectra changed dramatically upon oxygenation, indicating a strong change of the electronic structure of the complex. "Unspecific" oxidation of the macrocycle could be excluded, since the process was reversible and could be repeated multiple times if water was carefully removed from the solution.[24] Lubitz and co-workers studied oxygen adducts of H-capped cobaloxime in a zeolite matrix;[61] however, the X-band spectra presented previously exhibited rather low $g$-tensor resolution and did not allow a unique determination via magnetic parameters.

Here, we used the multifrequency approach described above to study the oxygenation of $Co(dmgBF_2)_2$. We choose a solvent mixture of toluene and $CH_2Cl_2$, which is known to solubilize $Co(dmgBF_2)_2$ well without exerting strong interactions on the cobalt center and also generates a good glass at cryogenic temperatures. These solvents have been previously used to study the oxygenation of cobalt complexes.[58−60] A small amount of $PPh_3$ was added to act as axial ligand for multiple reasons. In general, cobalt complexes without strong axial ligand are poor oxygen binders, whereas the presence of one strong axial ligand allows binding of molecular oxygen even at ambient pressures.[58] As mentioned above and observed previously,[26,29] the presence of $PPh_3$ in slight excess in the solution results exclusively in a singly ligated cobaloxime complex, displacing weakly interacting solvent molecules from one binding site and leaving the other coordination site open for another small ligand such as molecular oxygen. For the 2:1 ratio of $PPh_3$/cobaloxime investigated here, we observed quantitative binding of molecular oxygen as shown by the almost complete disappearance of the EPR signal typical for


dx.doi.org/10.1021/jp209395n | J. Phys. Chem. B 2012, 116, 2943−2957

anaerobic cobaloxime samples and appearance of an intense signal from the superoxide. This species was efficiently generated and rather stable in the presence of $PPh_3$, which is similar to the findings of Schrauzer and Lee for H-capped cobaloxime,[24] whereas the use of other axial ligands resulted in much lower yields of this paramagnetic species. Subsequent bubbling of the solution containing oxygenated cobaloxime with nitrogen gas largely restored the "original" signal as shown in Figure 2. These findings exclude the possibility that the cobaloxime has undergone unspecific oxidation of the macrocycle, which would instead show irreversible spectral changes. Prolonged incubation of the solution for days under aerobic conditions and ambient temperature lead to a steady decrease of the EPR signal, indicating slow degradation of the complex and buildup of possible diamagnetic dinuclear Co−$O_2$−Co complexes.[24,58] The presence of $^{31}P$ with a nuclear spin of $I$ = 1/2 as the ligating atom of $PPh_3$ also provides the advantage to monitor changes in the spin density distribution via $^{31}P$ hyperfine interaction with the unpaired electron(s) of the cobaloxime, but a possible shift of spin density to or from an axial ligand coordinating via an oxygen atom (i.e., acetone, methanol, or THF) cannot easily be observed.

The EPR spectra of oxygen-exposed $Co(dmgBF_2)_2$ recorded at the three different microwave frequencies are depicted in Figure 4. They are well resolved and could be simulated with the same set of parameters, indicating the presence of only one paramagnetic species. The D-band EPR spectrum (Figure 4a) is rather narrow (<0.15 T) as compared with the spectra of the Co(II) cobaloxime under anaerobic conditions (Figure 2). It exhibits the typical shape for a $S$ = 1/2 system with a rhombic $g$-tensor. In the following, we will keep the nomenclature introduced above to name the principal $g$ values as $g_x$ (for $g_{max}$), $g_y$ (for $g_{mid}$), and $g_z$ (for $g_{min}$). Note that different nomenclatures have been used previously.[60−62] In contrast to the spectra of the Co(II) cobaloxime recorded under anaerobic conditions, resolved hyperfine structure is not visible. The absence of the prominent cobalt hyperfine structure at the high-field part of the spectrum is a further indication of the significant electronic changes experienced by the cobalt ion upon binding of oxygen.

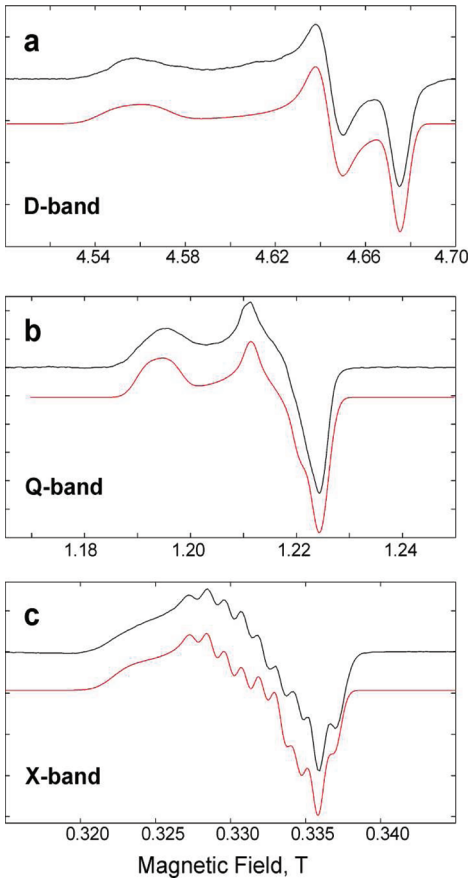


**Figure 4.** EPR spectra of the complex $PPh_3$:$Co(dmgBF_2)_2$ in a $CH_2Cl_2$/toluene 1:1 mixture under aerobic conditions recorded at different microwave frequencies (D-band, Q-band, X-band). The field-swept ESE-detected D-band spectra have been pseudomodulated. Q-band and X-band spectra are CW EPR spectra. Simulations are depicted in red.

The principal values of the $g$-tensor can be directly determined from the spectrum as 2.0390, 2.0014, and 1.9879. The $g$ values determined by Bakac et al. for acetone-ligated cobaloxime and by Schrauzer and Lee do not agree well with our findings.[24,25] This could be due to the difference in one of the axial ligands; however, the poorly resolved X-band EPR spectra reported previously might have resulted in an erroneous determination of the $g$-tensor. The pronounced reduction of the $g$-tensor anisotropy is typical for Co(II) low-spin complexes singly ligated by molecular oxygen.[58−60] At Q-band frequencies (Figure 4b), the spectrum is less than 40 mT wide, and the three principal $g$ values are still resolved, confirming the absence of any large hyperfine interaction. However, a clear broadening of the $g_y$ component can be observed, which can be attributed to unresolved hyperfine interaction.

At X-band frequency, the whole spectrum is ∼20 mT wide. Its appearance resembles many X-band spectra of oxygenated forms of related cobalt complexes and cobaloximes (see, e.g., refs 60, 63, 64 ). A well-resolved hyperfine structure is visible around $g_y$, although the hyperfine structure around $g_x$ is not resolved. This is in contrast to vitamin $B_{12}$ complexes, in which the hyperfine structure at low field is typically well resolved.[61,64,65] The number of lines could only be reproduced in the spectral simulation by the assumption of significant hyperfine interaction of one phosphorus nucleus and one cobalt nucleus, both being very similar in magnitude, around 35 MHz. The presence of substantial $^{31}P$ hyperfine interaction was confirmed by additional experiments. The use of PDI instead of $PPh_3$ as the axial ligand resulted in a decrease in hyperfine lines from nine to eight (see Figure S7 of the Supporting Information).

The absence of a visible hyperfine structure at $g_x$ allows no reliable estimation of $A_x$ for either $^{59}Co$ or $^{31}P$. The EPR signals arising from $g_z$ severely overlap with the hyperfine structure of $g_y$. The $A_x$ and $A_z$ values used for the simulation thus bear a rather large error. The much lower magnitude of the $^{31}P$ hyperfine interaction as compared with the deoxygenated cobaloxime is in line with the observed dramatically reduced $^{59}Co$ $A$ values due to the lower spin density on the coordinated cobalt ion. In this type of complex, the $^{59}Co$ $A$-tensor and $^{31}P$ $A$-tensor are expected not to be collinear anymore with the $g$-tensor.[60] Lifting the assumption of collinear axes systems and using angles similar to those in studies of related cobalt oxygen adducts[60,63,65] lead only to minor changes in the spectral simulations. Schrauzer and Lee estimated for the H-capped cobaloxime a reduction of unpaired spin density at the cobalt by at least a factor of 5 on the basis of the $^{59}Co$ isotropic


dx.doi.org/10.1021/jp209395n | J. Phys. Chem. B 2012, 116, 2943−2957

**Table 2. Conformations, Energies, Cobalt out-of-Plane Distances, and Magnetic Parameters for the Cobaloxime $Co(dmgBF_2)_2$ Obtained by DFT Calculations[a]**

| complex | conformation | Co out-of-plane distance (Å)[b] | energy of complex formation (kcal/mol)[c] | g values | $A(^{59}Co)$ (MHz) | ligand superhyperfine $A(^{14}N)$ (MHz) or $A(^{31}P)$ (MHz) |
|---|---|---|---|---|---|---|
| pyrdine:Co (2:1) | boat | 0.15 | −25.8 | 2.1382, 2.0980, 2.0057 | −99, −139, +359 | +37(+37), +38(+38), +46(+47) |
| | chair | 0.03 | +2.34 | 2.0362, 2.0157, 1.9972 | −152, −5, +11 | +26(+29), +30(+33), +63(+65) |
| | exp | | | 2.1910, 2.1270, 2.0080 | 105, 148, 242 | 36 39 48 |
| pyridine:Co (1:1) | chair | 0.27 | −26.8 | 2.2074, 2.1387, 2.0074 | −52, −69, +355 | +29, +30, +36 |
| | boat toward | 0.32 | −25.4 | 2.2043, 2.1266, 2.0073 | −71, −91, +345 | +28, +29, +37 |
| | boat away | 0.18 | −24.2 | 2.1890, 2.1303, 2.0071 | −46, −61, +368 | +29, +30, +37 |
| | exp | | | 2.2380, 2.1530, 2.0058 | 10, 10, 285 | 33, 36, 43 |
| PDI:Co (2:1)[d] | boat | 0.14 | −21.4 | 2.1413, 2.1008, 2.0054 | −85, −126, +369 | +37(+37), +37(+38), +46 (+46) |
| PDI:Co (1:1)[d] | boat away | 0.18 | −25.6 | 2.1910, 2.1323, 2.0069 | −38, −55, +375 | +29, +30, +38 |
| | boat toward | 0.14 | −23.6 | 2.2074, 2.1290, 2.0071 | −66, −88, +348 | +28, +29, +37 |
| | chair | 0.28 | −23.3 | 2.2183, 2.1549, 2.0076 | +9, +28, +423 | +28, +29, +36 |
| | exp | | | 2.3473, 2.1815, 2.0000 | 85, 10, 306 | 30, 30, 40 |
| methanol:Co (2:1) | chair | 0.00 | −24.5 | 2.1535, 2.1153, 2.0052 | −27, −61, +423 | n/a |
| | boat | 0.08 | −23.0 | 2.1626, 2.1212, 2.0057 | −11, −41, +435 | n/a |
| | exp | | | 2.2840, 2.1820, 2.0080 | 53, 20, 338 | n/a |
| methanol:Co (1:1) | chair | 0.17 | −22.1 | 2.2215, 2.1564, 2.0066 | +59, +39, +456 | n/a |
| | boat toward | 0.27 | −21.8 | 2.2338, 2.1564, 2.0070 | +34, +14, +427 | n/a |
| | boat away | 0.34 | −14.8 | 2.2728, 2.2116, 2.0084 | −19, −38, +335 | n/a |
| $H_2O$:Co (2:1) | chair | 0.00 | −25.0 | 2.1529, 2.1159, 2.0053 | −29, −64, +424 | n/a |
| | boat | 0.06 | −23.8 | 2.1507, 2.1158, 2.0054 | −40, −72, +418 | n/a |
| | exp | | | 2.2750, 2.1785, 2.0065 | 15, 15, 329 | n/a |
| $H_2O$:Co (1:1) | boat toward | 0.23 | −22.4 | 2.2158, 2.1527, 2.0067 | +28, +13, +436 | n/a |
| | boat away | 0.10 | −21.0 | 2.2195, 2.1629, 2.0068 | +94, +69, +486 | n/a |
| | chair | 0.39 | −2.2 | 2.3146, 2.1604, 2.0093 | −27, −59, +311 | n/a |
| methanol:Co:pyridine (1:1:1) | boat-methanol | 0.03 | −26.4 | 2.1452, 2.1056, 2.0056 | −79, −108, +375 | +35, +36, +44 |
| | chair | 0.13 | −25.0 | 2.1500, 2.1109, 2.0056 | −101, −66, +385 | +34, +35, +43 |
| | boat-pyridine | 0.21 | −24.2 | 2.1551, 2.1076, 2.0057 | −89, −118, +367 | +34, +35, +43 |
| $PPh_3$:Co (2:1) | chair | 0.00 | −10.9 | 2.2070, 2.1431, 2.0060 | +120, +164, +527 | +251, +252, +308 |
| $PPh_3$:Co (1:1) | boat away | 0.22 | −18.9 | 2.2213, 2.1455, 2.0072 | +49, +19, +408 | +236, +235, +283 |
| | chair | 0.28 | −18.0 | 2.2318, 2.1481, 2.0073 | +38, +6, +396 | +241, +240, +290 |
| | boat toward | 0.32 | −12.6 | 2.2467, 2.1574, 2.0075 | +43, +16, +400 | +254, +253, +307 |
| | exp | | | 2.3000, 2.1425, 1.9995 | 36, 10, 249 | 300, 300, 358 |
| $PPh_3$:Co:$O_2$ (1:1:1)[e] | chair | 0.10 | −46.6 | 2.0462, 2.0062, 1.9908 | −50, −30, −21 | −15, −15, −15 |
| | boat-$PPh_3$ | 0.13 | −45.8 | 2.0357, 2.0005, 1.9829 | −78, −34, −30 | −15, −19, −19 |
| | boat-$O_2$ | 0.07 | −47.8 | 2.0454, 2.0062, 1.9912 | −48, −28, −19 | −15, −15, −15 |
| | exp | | | 2.0390, 2.0014, 1.9879 | 28, 32, 13 | 20, 37, 37 |

[a]The calculations of magnetic parameters were performed on the geometry optimized structures (see Experimental Procedures for details). The magnetic dipole and the isotropic Fermi contact hyperfine coupling constants were calculated for all atoms, and for $^{59}Co$, second-order spin-orbit hyperfine contributions are also included. The $^{14}N$ hyperfine coupling constants refer to the axial ligands, not to the macrocycle (equatorial) nitrogen atoms. Values in parentheses are provided if the two axial nitrogen atoms are magnetically not equivalent. [b]The cobalt out-of-plane distance is measured from the cobalt atom to the center of a plane formed between the four nitrogen atoms in the cobaloxime structure. [c]Energy of complex formation: The energies of complex formation are estimated from subtracting the energies of the individual geometry optimized substituents (ligands and cobaloxime) from the energy of the geometry optimized complex. The energies include contributions from the COSMO solvent effect. [d]For PDI as the axial ligand, the geometry optimizations were performed with the complete molecule; the magnetic parameter calculations were performed with a truncated PDI model system. [e]In this complex, the principal axes of the *g*-tensor and the hyperfine tensors/*A*-tensors deviate with respect to each other and the molecular axes system. The respective Euler angles are provided in Table S3 in the Supporting Information.

hyperfine coupling. Even larger reductions have been estimated for H-capped cobaloxime[61] and related compounds.[63,65]

Cobalt complexes can form several different complexes with molecular oxygen (see, e.g., ref 58). One complex that may be formed by cobaloximes dissolved in organic solvents in the presence of molecular oxygen is dinuclear $\mu$-peroxides, as shown previously for H-capped cobaloxime.[24] This type of dinuclear complex is diamagnetic and, thus, not detectable by EPR spectroscopy. A paramagnetic $\mu$-superoxo radical cation $L-Co(dmg_2H_2)-O_2-Co(dmg_2H_2)-L^+$ with a characteristic 15-line signal in liquid solution was also observed. This signal is due to the interaction of two magnetically equivalent cobalt nuclei with the unpaired electron symmetrically delocalized over the $Co-O_2-Co$ moiety.[24] We did not observe the dinuclear $\mu$-superoxo radical under our experimental conditions. Mononuclear superoxide complexes can be described as


dx.doi.org/10.1021/jp209395n | J. Phys. Chem. B 2012, 116, 2943−2957

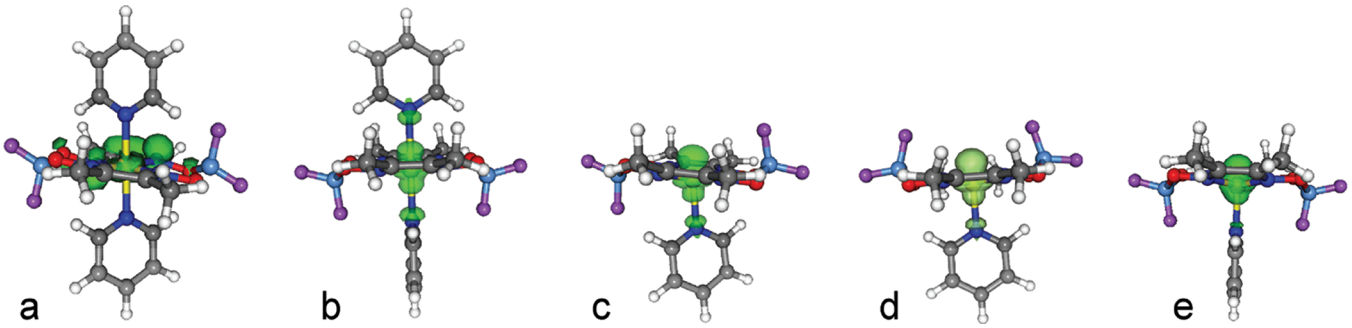


**Figure 5.** Spin density isosurface plots of cobaloxime $Co(dmgBF_2)_2$. All isosurfaces are shown at a contour level of 0.005 $e/a_0^3$. From left to right: (a) Doubly ligated by pyridine (chair), (b) doubly ligated by pyridine (boat), (c) singly ligated by pyridine (chair), (d) singly ligated by pyridine (boat away), and (e) singly ligated by pyridine (boat toward).

$L-Co(dmg_2H_2)-O_2^{\bullet}$ and characterized by a hyperfine splitting multiplicity of 8, indicative of the presence of only one cobalt ion in the complex. This complex was obviously observed in our study. The frozen solution spectra reported here show no indication of $S > 1/2$. Because Co(II) has one unpaired electron in the nonoxygenated complex, and molecular oxygen is a ground state triplet ($S = 1$) due to two unpaired electrons, the resultant spin is $S = 1/2$.

The coordination environment in Co(II) Schiff base compounds resembles that of cobaloxime, and a qualitative interpretation of the EPR spectra of these compounds binding molecular oxygen has been given by Hoffman et al.[63] In that work, the authors concluded that the cobalt ion is essentially oxidized to Co(III) and the molecular oxygen is reduced to the superoxide ion, $O_2^-$, and estimated the transfer of spin density from cobalt to oxygen to be roughly 90%. Schrauzer and Lee determined the $^{59}$Co isotropic hyperfine coupling for the H-capped cobaloxime and estimated a reduction of unpaired spin density at the cobalt by a factor of 5−10. Since we observe similar hyperfine coupling for the difluoroboryl cobaloxime, we may follow their line of reasoning. Additional experimental evidence that related cobalt complexes form under the presence of molecular oxygen Co(III) superoxide complexes provides further support of an assignment of our complex as being formally $LCo(III)O_2^{\bullet}$ superoxide.[58,59,61,65−67]

We thus conclude that there is almost complete transfer of the cobaloxime's unpaired electron spin density to the oxygen. The $g$-tensor anisotropy is then mostly determined by the spin density on the oxygen atoms, and the principal component of the $g$-tensor with the largest deviation from $g_e$ will be in the direction of the interoxygen axis. The cobalt hyperfine coupling instead is determined by the 3d orbital of the cobalt ion, and this presents a pronounced difference to the nonoxygenated complex. From our experimental data, no direct conclusion is possible regarding the presence of the three different conformers (chair, boat-$PPh_3$, boat-$O_2$). A comparison with the results from the DFT calculation let us favor the boat-$PPh_3$ conformation (see discussion below).

## DFT RESULTS

The calculated $g$ values, $^{59}$Co $A$ values, and superfine coupling constants are presented in Table 2. To the best of our knowledge, these are the first published EPR parameter calculations for singly and doubly ligated Co(II) cobaloxime complexes. Previous semiempirical calculations focused on the effect of the cobalt displacement on the energetics of the compound[29] and four-coordinate Co(II) complexes without axial ligands being reported.[68] Recent DFT studies on cobaloxime did not report any magnetic parameters.[69,70] The structure of the cobaloxime complex allows multiple conformations of each cobaloxime−ligand(s) complex. As shown in Figure 5, using the common cyclohexane notation, the conformations can be labeled "chair" and "boat" with the possibility of further specifying the boat as toward or away from the attached ligand. If only one axial ligand molecule was included in the calculation, the expressions "boat toward ligand" or "boat away" are used. The "boat" and "chair" conformations refer to the orientations of the $BF_2$ caps with respect to the macrocycle plane. Unlike the four-coordinate Co(II) complexes investigated by Zbiri,[68] our calculated $g$ values do not change significantly when other hybrid functionals are used. Before discussing in detail the results of the calculations, some critical issues regarding the accuracy and reliability of the calculations are addressed briefly.

One problem of DFT calculations on large, open-shell transition metal complexes is the high accuracy required to distinguish among conformations that are quite close in energy as compared with the overall energy of the complex. This is partially the result of inherent approximations made in DFT calculations.[71,72] At least part of the discrepancy between actual and calculated energies is due to insufficient inclusion of the interactions with solvent. Increasing the number of solvent molecules in the calculation and thus forming an extended solvent shell around the complex may lead to an improved prediction of conformational energies and also to improved magnetic parameters as compared with pure gas phase calculations.[73−75] However, the explicit inclusion of a large number of solvent molecules is computationally demanding; thus, such time-consuming calculations were not performed. Instead, only the direct ligands to the central cobalt atom were explicitly included, and the residual surrounding solvent molecules were implicitly included using the dielectric screening model COSMO.[44] This neglect is considered to be most problematic for those solvent molecules in which significant direct interactions with the cobaloxime are expected. For example, it has been shown that hydrogen bonding is in many cases essential to geometries and electronic structures.[76−78] However, since in our study the experimental spectra of cobaloxime in methanol/pyridine and acetone/pyridine mixtures were almost identical (see Table 1 for the magnetic parameters), possible hydrogen bonding to the cobaloxime by solvent molecules is not considered critical for the electronic structure of the cobalt complex, and thus, no


dx.doi.org/10.1021/jp209395n | J. Phys. Chem. B 2012, 116, 2943−2957

calculations with solvent molecules ligated to the fluorine atoms were performed.

If conformers exist with comparable energies (same order of magnitude as kT), the complexes in frozen solution studied by EPR spectroscopy may also consist of a mixture of conformers trapped during the freezing process. In addition, our calculations determine the energetic minimum but do not include entropic contributions. Hence, instead of choosing only the lowest-energy conformation, we present the magnetic parameters calculated for the various conformations. It is expected that the comparison with the experimentally determined magnetic parameters allows us to more reliably exclude conformers than a discrimination based solely on energy. To validate the quality of the geometry optimization, we repeated selected calculations with different functionals, basis sets, and dielectric constants. Use of a sufficiently large dielectric constant for the COSMO screening model was found to be needed to obtain reasonable structures, that is, to avoid structures with strong distortion of the macrocycle. Otherwise, all calculations resulted in nearly identical geometries and energetic orderings within the conformations, which suggests that the obtained structures are reliable. Problems with precisely calculating the magnetic parameters for our specific transition metal complexes are discussed below in relation to the available experimental data.

**Cobaloxime with Axial Ligands (except Molecular Oxygen).** As shown in Table 2, the position of the cobalt with respect to the plane of the cobaloxime macrocycle varies greatly, depending on the number and nature of the axial ligand(s). Most notably, the diwater and dimethanol complexes result in the cobalt remaining nearly planar and the nitrogen and phosphorus containing ligands pull the cobalt out of plane. In addition, singly ligated complexes pull the cobalt out of the plane to a greater degree than their doubly ligated counterparts, and the boat conformations show greater displacements than the chair.

To evaluate systematically the effect of this cobalt out-of-plane movement on the electronic $g$-tensor and the cobalt hyperfine interaction independent of the chemical nature of the ligand, we investigated a model system composed of just the cobaloxime with one pyridine molecule in the "boat toward pyridine" conformation. The energetic minimum for this system has the Co(II) ion located 0.327 87 Å below the plane of the macrocycle pulled toward the pyridine. In these calculations, the cobalt atom was moved in and out of the macrocycle nitrogen plane fixed there while the rest of the molecule was allowed to relax. Further details of the calculation are given in the Experimental Procedures section. The effects on the $g$ values and $^{59}$Co hyperfine coupling constants $A_x$, $A_y$, and $A_z$ are presented in Figure 6 and listed in Table S1 of the Supporting Information. In the case without forced displacement of the Co(II) ion, the principal $g$ values, $^{59}$Co $A$ values, and $^{14}$N $A$ values resemble those obtained experimentally. The displacement of the cobalt ion leads to a systematic change in both the principal $g$ values and the $^{59}$Co $A$ values, but the $^{14}$N $A$ values (not shown) do not appreciably vary from the nondisplaced case. Notably, the $^{59}$Co $A$ values exhibit an almost linear relationship with cobalt out-of-plane distance. $A_x$, $A_y$, and $A_z$ values all decrease as the cobalt moves farther away from the plane. Moving the Co(II) ion into the plane, beyond the energetic minimum position, has a weak influence on the $g$ values. Despite the correlation shown in the test calculation, the chemical nature of the ligand and the chair/boat conformation

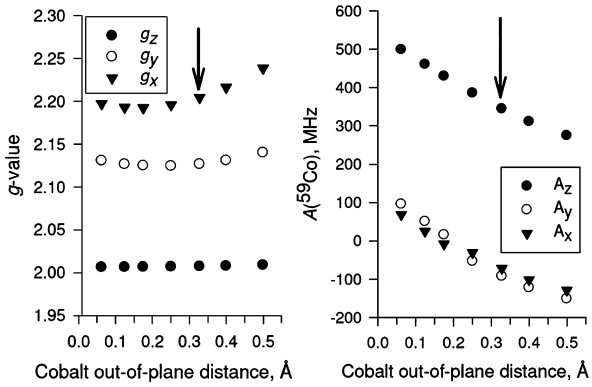


**Figure 6.** Effect of cobalt out-of-plane distance on electronic $g$ values $g_x$ (▼), $g_y$ (○), and $g_z$ (●) and $^{59}$Co hyperfine coupling constants $A_x$ (▼), $A_y$ (○), and $A_z$ (●) for Co(dmgBF$_2$)$_2$. The complex contains a single pyridine molecule as the axial ligand in the "boat toward pyridine" conformation. A restricted geometry optimization was performed with the Co(II) ion pulled systematically in and out of the plane of the macrocycle (as compared with the calculation without constraint with a out-of-plane distance of 0.327 87 Å) using a torsion constraint (Co−N−N−N, Figure 1). The $^{14}$N $A$ values of the axial pyridine ligand do not appreciably vary from the case without constraints (data not shown). Details of the DFT calculations are given in the Experimental Procedures section. For both graphs, the arrows mark the unconstrained optimized structure. The numerical values are given in Table S1 (Supporting Information).

seems to obscure this effect on the values of the principal $g$ and $^{59}$Co $A$ values. Thus, it is not possible to directly predict the cobalt position from the $g$ or $^{59}$Co $A$ values.

For example, consider the singly ligated water case (Table 2). The two boat conformations differ in the cobalt distance by 0.13 Å, and the $^{59}$Co $A_z$ values decrease, as expected. The chair conformation has an even larger distortion and a concurrent larger drop in the $^{59}$Co $A_z$ value; however, the $g$ values do not increase for the chair conformation, as might have been expected from the model. In general, the $^{59}$Co $A_z$ values are most sensitive to the cobalt position, whereas the $g$ values are a poor indicator of cobalt position. This is in agreement with prior work on $d^1$ five-coordinate systems that showed only a weak dependence of the $g$ values on geometry.[79] In terms of directly predicting the experimental $g$-tensor, the calculations correctly reproduce the trend of decreasing $g$ values ($g_x$, $g_y$) as the complex goes from singly ligated by pyridine to doubly ligated. However, the calculations underestimate the $g_x$ value for all ligands except the $PPh_3$ oxygen adduct. This is not a problem specific to our study. The systematic underestimation of $g$ values of transition metal complexes by DFT is common;,[72] nevertheless, they can be used to indicate a trend within the series of calculations.

Turning to the $^{59}$Co $A$ values, qualitative rather than quantitative agreement is present. The three contributions to the (transition metal) hyperfine interaction (Fermi contact, spin-dipolar, and spin-orbit coupling) are known to be difficult to calculate with accuracy.[80,81] In agreement with experiment, the $A_z$ values of Co(dmgBF$_2$)$_2$ in methanol and water are greater than the corresponding values for pyridine.

The $^{14}$N $A$ values of the equatorial (dimethylglyoxime) nitrogen atoms were also calculated. They are found to be small, below 8 MHz in all (energetically reasonable) cases, and in a majority of cases, well below that (see Table S2 of the Supporting Information). The hyperfine coupling constants of


dx.doi.org/10.1021/jp209395n | J. Phys. Chem. B 2012, 116, 2943−2957

the equatorial nitrogen atoms were not resolved in the EPR spectra. HYSCORE data of $Co(dmgBF_2)_2$ in methanol (see Figure S6 of the Supporting Information) allows us to estimate these $^{14}N$ hyperfine coupling constants as below 4 MHz, which is in a good agreement with the principal values obtained by the DFT calculation. The $^{14}N$ and $^{31}P$ *A* values of the axial ligands that could be determined from the EPR spectra were nicely reproduced by the DFT calculations (see Tables 1 and 2). The general better agreement of superhyperfine interactions than hyperfine interactions of the central metal ion is typical for DFT calculations.[82]

The binding energies for the six-coordinate complexes (two axial ligands) predicted by the calculations are in general agreement with experiments (pyridine > methanol; $PPh_3$ > toluene, $CH_2Cl_2$). In some of these cases, the singly ligated conformation appears to be more energetically favorable than the doubly ligated one. As noted previously, some ligands, such as $PPh_3$ seem to result in a stabilization of the singly ligated Co(II) complex.[29] Prior authors attributed this observation to a distortion of the cobaloxime structure in which the Co(II) is pulled out of the plane toward the ligand and the equatorial glyoxime ligands are folded away from the axial ligand. By comparing binding energies, it is clear that although water and methanol are more stable as doubly ligated complexes, this is not true for other complexes. The pyridine complex is nearly isoenergetic as a 2:1 and a 1:1 complex whereas the calculations predict that the $PPh_3$ and PDI complexes prefer the monosubstituted complex. These results are in good agreement with the experimental results.

For PDI and $PPh_3$ we observed only singly ligated complexes, and already a moderate excess of pyridine leads to a significant presence of doubly ligated complexes. However, the optimized structures of complexes singly ligated by pyridine or PDI are very similar and yield similar magnetic parameters, whereas the latter is not found experimentally. From calculations, it is unclear whether a solvent effect is present (methanol or acetone for pyridine, and toluene or $CH_2Cl_2$/toluene for PDI and $PPh_3$). It seems likely that for cobaloxime singly ligated by pyridine in the methanol solution, a methanol molecule acts as a second but "weak" ligand.

Computationally, the binding of a single PDI molecule to the cobalt induces out-of-plane displacements almost identical to that of the binding of pyridine. Experimentally, the single PDI molecule binding results in the largest $g_x$ value; however, in the DFT calculation, this large *g*-tensor anisotropy is not reproduced. In fact, not surprisingly, the calculated magnetic parameters of cobaloxime singly ligated by one PDI molecule resemble relatively closely those of cobaloxime singly ligated by pyridine (Table 2). This might be explained by our tentative assumption that the quite nonpolar solvents (toluene or $CH_2Cl_2$/toluene mixture) have an additional effect on the geometry and electronic structure of the cobaloxime complex (see above). For PDI in neat toluene, the second axial ligand may be either absent or hardly coordinating, in contrast to methanol or acetone as solvents. This might be especially prominent, since both PDI and $PPh_3$ are the most bulky ligands studied here. A highly simplified picture would be a kind of "folding" of the macrocycle; however, computationally, optimizing the singly ligated PDI complex using a low dielectric constant but not explicitly solvent molecules does not appreciably change the geometry or the *g* values.

Experimentally, the single $PPh_3$ ligand results in the second-largest $g_x$ component determined, but in a rather small $g_y$ value. Although the geometry of the singly ligated $PPh_3$ complex after energetic minimization is quite distorted, the calculations still underestimate $g_x$ but match $g_y$ quite well.

In addition to influencing the location of the cobalt atom, the ligands also seem to influence the stability of the boat/chair conformational preference of the cobaloxime itself. In particular, water and methanol are most stable in the chair conformation shown in Figure 5, whereas pyridine is most stable in the boat conformation (Table 2). The "chair" structure obtained for two methanol ligand molecules is in good agreement with the crystal structure determined by Bakac et al.[25] Our calculated structure has a cobalt−methanol oxygen distance of 2.246 Å, and the crystal structure reports a distance of 2.264(4) Å. Within this work, the crystal structure of $Co(dmgBF_2)_2$ with two acetonitrile molecules as ligands was determined (see Supporting Information). It exhibits a similar distance with 2.25 Å and also shows "chair" conformation. Both the calculated and the two crystal structures have in-plane cobalt atoms. Although no dipyridine crystal structure exists, support for the boat structure is evident both in the energetics and in the *g*-and *A* values.. The calculations also predict that PDI would exhibit the boat conformation. For the $PPh_3$:Co (1:1) complex, the energetics suggest that the "boat toward" conformers is less likely, but all three conformers have magnetic parameters so similar that we cannot distinguish them with reference to the experimental data.

The DFT calculations provide not only the magnitude of the magnetic interactions but also the orientation of the *g*-tensor principal axes and those of the *A*-tensors ($^{59}Co$, $^{14}N$, $^{31}P$) within the molecular frame. Figure 1 presents the molecular axes system of cobaloxime, with the axes labeled accordingly. For all cases without molecular oxygen bound to the Co(II) ion, we observed that the lowest *g* value, $g_z$, is perpendicular to the equatorial plane, that is, pointing along the $d_{z2}$ orbital. The middle *g*-value, $g_y$, is always found to be collinear to the boron−boron axis, and the highest *g*-value, $g_x$, is perpendicular to the other two. The $^{59}Co$ *A*-tensor principal axes are also to a good approximation collinear to the molecular axes system. The deviation of the electronic *g*-tensor and $^{59}Co$ *A*-tensor from the molecular axes system was usually <5°. Only the binding of $PPh_3$ which caused a slight distortion of the macrocycle, resulted in deviations up to 10°. All ligands' ($^{14}N$, $^{31}P$) *A*-tensors were collinear to the molecular axes system with deviations of <5°.

**Cobaloxime with Oxygen and $PPh_3$ As Axial Ligands (Molecular Oxygen Adduct).** Finally, DFT calculations on the $O_2$:Co:$PPh_3$ complex were done for the three conformers: chair, boat toward $PPh_3$, and boat toward $O_2$. All three conformers are rather close in energy (Table 2). Geometry optimizations were performed several times with different starting structures that differed regarding the orientation of the oxygen molecule with respect to the cobaloxime. All calculations resulted in the O−O−Co angle remaining near 120°. For the conformers chair and boat toward $PPh_3$, the minimum is very shallow (<2 kcal/mol as the $O_2$ is rotated over the macrocycle). In contrast, the boat toward $O_2$ structure results in structures with unbound oxygen if the initial O−O−Co−N dihedral angle deviates from the one found in the energetic minimum. For all three, the magnetic parameters exhibit no pronounced differences and show reasonable agreement with the experiment regarding the electronic *g*-tensor, the $^{59}Co$ *A*-tensor, and the $^{31}P$ *A*-tensor. However, the *g*-tensor of the "boat toward $PPh_3$" conformer shows the best


dx.doi.org/10.1021/jp209395n | J. Phys. Chem. B 2012, 116, 2943−2957

agreement with the experiment, and we discuss this boat conformer in the following.

The analysis of the other conformers is similar. In the "boat toward $PPh_3$" conformer, the distance between cobalt and the bound phosphorous atom is 2.57 Å and, hence, hardly changed as compared with the corresponding 2.63 Å found in the deoxygenated complex. The distance between the two oxygen atoms is 1.35 Å. The calculated distance between the two oxygen atoms of unbound molecular oxygen is 1.22 Å, whereas the calculated distance in $O_2^-$ is 1.35 Å (both distances from DFT calculations with 6-31G* basis set). The virtually identical distance between the two oxygen atoms in the oxygen adduct and the $O_2^-$ anion is a strong hint that a substantial shift of the electron density from cobalt toward the oxygen has occurred and, thus, supports the formal description of the oxygen adduct as a $LCo(III)O_2^-$ superoxide. The Co−O−O bond angle is 119°, which is in the typical range found for cobalt superoxide complexes.[58] In addition, the spin density (shown in Figure 7)

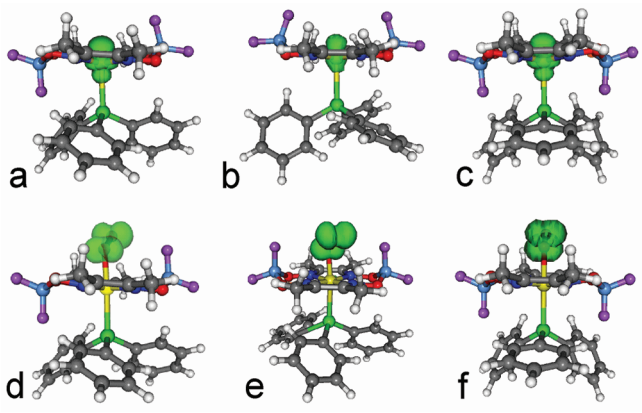


**Figure 7.** Spin density isosurface plots of cobaloxime $Co(dmgBF_2)_2$. All isosurfaces are shown at a contour level of 0.005 $e/a_0^3$: (top) the complex $PPh_3$:Co (1:1) in (a) "chair", (b) "boat away", and (c) "boat toward" conformation and (bottom) the complex $PPh_3$:Co:$O_2$ (1:1:1) in (d) "chair", (e) "boat toward $O_2$", and (f) "boat toward $PPh_3$"conformation.

exhibits the expected shift from the Co(II) ion to the $O_2$ molecule. This calculation thus clearly refutes for the cobaloxime the spin-pairing model proposed by Tovrog et al.[83,84] and supports the view of the oxygen adduct as a $LCo(III)O_2^\bullet$ superoxide. The principal axes of the *g*-tensor and the *A*-tensors ($^{59}$Co and $^{31}$P) deviate with respect to each other and the molecular axes system (see Table S3 in the Supporting Information). This is typical for $O_2$:Co:L complexes.[60,62,63,65]

## CONCLUSION

In conclusion, we have presented a comprehensive study of the molecular $H_2$ catalyst $Co(dmgBF_2)_2$ by multifrequency EPR spectroscopy at X-band (9 GHz), Q-band (34 GHz), and D-band (130 GHz) combined with DFT calculations. Cobaloxime was investigated in a number of solvents with different polarity, proticity, and stochiometric amounts of potential ligands to the cobalt ion. This approach allows a clear distinction among labile and strongly coordinating types of axial ligands to the Co(II) macrocycle as well as two types of strong Co(II) coordination: singly ligated $LCo(dmgBF_2)_2$ and doubly ligated $L_2Co(dmgBF_2)_2$. Weakly coordinating ligands such as methanol result in larger *g*-tensor anisotropy than strongly coordinating ligands such as pyridine. The presence of two strongly coordinating axial ligands leads to the smallest *g*-tensor anisotropy. Strongly binding N-donating solvents displace the weaker O-donating solvents as axial ligands to the Co(II) ion in the cobaloxime. Therefore, O-donating solvent environments can more readily facilitate proton binding at the cobalt center to initiate H−H bond formation, rather than forming a tight and rather stable complex with solvent molecules and hindering proton binding. The influence of molecular oxygen and formation of Co(III) superoxide radicals $LCo(dmgBF_2)_2O_2^\bullet$ was also studied. The proportional decrease in both ligand and $^{59}$Co hyperfine coupling constants for the reversible $LCo(dmgBF_2)_2 + O_2 \leftrightarrows LCo(dmgBF_2)_2O_2^\bullet$ transformation is consistent with a substantial shift of electron spin density to oxygen. Finally, the results obtained experimentally are compared with a comprehensive set of DFT calculations on $Co(dmgBF_2)_2$ model systems with various axial ligands and on oxygen adducts in the presence of $PPh_3$. Comparison with experimental values for the "key" magnetic parameters such as *g*-tensor and $^{59}$Co *A*-tensor allows the determination of the identity of the ligands and conformation of the axially ligated $Co(dmgBF_2)_2$ complexes.

In this study, we chose this $BF_2$-capped cobaloxime in particular because it stands out among earth-abundant $H_2$ catalysts as extremely efficient and quite stable under relevant conditions for catalysis. Our observations provide important insight into electro- and photocatalytic efficiencies and explain, for example, the results of Fihri et al. on supramolecular cobaloxime photocatalysis, who found a nearly 6-fold enhancement in $H_2$ turnovers in acetone solution as compared with acetonitrile.[4]

Future work will be directed toward understanding the catalytical activity of supramolecular assemblies of cobaloxime as catalyst and photosensitizers, including conventional artificial photosensitizers as well as natural photosentizers (i.e., photosynethetic proteins).[85] We anticipate that the combination of multifrequency EPR structural analysis and high-level DFT calculations will provide a predictive role in the development of new photocatalysts.

## ASSOCIATED CONTENT

### Supporting Information

Molecular structures, EPR, HYSCORE, and ENDOR spectra of $Co(dmgBF_2)_2$ in various solvents and under different experimental conditions. Additional results of DFT calculations. Crystal structure of $Co(dmgBF_2)_2$ used for geometry optimization calculations (CIF file and checkCIF file). This material is available free of charge via the Internet at http://pubs.acs.org.

## AUTHOR INFORMATION

### Corresponding Author

*E-mail: Jniklas@anl.gov (J.N.), Oleg@anl.gov (O.G.P.).

## ACKNOWLEDGMENTS

This work was supported by the U.S. Department of Energy, Office of Basic Energy Sciences, Division of Chemical Sciences, Geosciences, and Biosciences, under Contract DE-AC02-06CH11357. K.L.M. thanks the National Institutes of Health (Grant 1SC2GM083717) and the National Science Foundation IL-LSAMP Grant HRD-0413000.

## REFERENCES


(1) Lewis, N. S.; Nocera, D. G. *Proc. Natl. Acad. Sci. U.S.A.* **2006**, *103*, 15729−15735.
(2) Cook, T. R.; Dogutan, D. K.; Reece, S. Y.; Surendranath, Y.; Teets, T. S.; Nocera, D. G. *Chem. Rev.* **2010**, *110*, 6474−6502.
(3) Dempsey, J. L.; Brunschwig, B. S.; Winkler, J. R.; Gray, H. B. *Acc. Chem. Res.* **2009**, *42*, 1995−2004.
(4) Fihri, A.; Artero, V.; Razavet, M.; Baffert, C.; Leibl, W.; Fontecave, M. *Angew. Chem., Int. Ed.* **2008**, *47*, 564−567.
(5) Schrauzer, G. N.; Windgassen, R. J. *J. Am. Chem. Soc.* **1966**, *88*, 3738−3743.
(6) Schrauzer, G. N.; Sibert, J. W.; Windgassen, R. J. *J. Am. Chem. Soc.* **1968**, *90*, 6681−6688.
(7) Schrauzer, G. N. *Angew. Chem., Int. Ed.* **1976**, *15*, 417−426.
(8) Banerjee, R. *Chemistry and Biochemistry of B12*; J. Wiley & Sons: New York, 1999.
(9) Kräutler, B.; Arigoni, D.; Golding, B. T. *Vitamin B12 and B12-Proteins*, Wiley-VCH: Weinheim, 1998.
(10) Connolly, P.; Espenson, J. H. *Inorg. Chem.* **1986**, *25*, 2684−2688.
(11) Hu, X. L.; Cossairt, B. M.; Brunschwig, B. S.; Lewis, N. S.; Peters, J. C. *Chem. Commun.* **2005**, 4723−4725.
(12) Baffert, C.; Artero, V.; Fontecave, M. *Inorg. Chem.* **2007**, *46*, 1817−1824.
(13) Hu, X. L.; Brunschwig, B. S.; Peters, J. C. *J. Am. Chem. Soc.* **2007**, *129*, 8988−8998.
(14) Razavet, M.; Artero, V.; Fontecave, M. *Inorg. Chem.* **2005**, *44*, 4786−4795.
(15) Lazarides, T.; McCormick, T.; Du, P. W.; Luo, G. G.; Lindley, B.; Eisenberg, R. *J. Am. Chem. Soc.* **2009**, *131*, 9192−9194.
(16) McCormick, T. M.; Calitree, B. D.; Orchard, A.; Kraut, N. D.; Bright, F. V.; Detty, M. R.; Eisenberg, R. *J. Am. Chem. Soc.* **2010**, *132*, 15480−15483.
(17) Dempsey, J. L.; Winkler, J. R.; Gray, H. B. *J. Am. Chem. Soc.* **2010**, *132*, 16774−16776.
(18) Zhang, P.; Wang, M.; Dong, J. F.; Li, X. Q.; Wang, F.; Wu, L. Z.; Sun, L. C. *J. Phys. Chem. C* **2010**, *114*, 15868−15874.
(19) Wang, M.; Na, Y.; Gorlov, M.; Sun, L. C. *Dalton Trans.* **2009**, 6458−6467.
(20) Fihri, A.; Artero, V.; Pereira, A.; Fontecave, M. *Dalton Trans.* **2008**, 5567−5569.
(21) Mulfort, K. L.; Tiede, D. M. *J. Phys. Chem. B* **2010**, *114*, 14572−14581.
(22) Li, C.; Wang, M.; Pan, J. X.; Zhang, P.; Zhang, R.; Sun, L. C. *J. Organomet. Chem.* **2009**, *694*, 2814−2819.
(23) Bakac, A.; Espenson, J. H. *J. Am. Chem. Soc.* **1984**, *106*, 5197−5202.
(24) Schrauzer, G. N.; Lee, L. P. *J. Am. Chem. Soc.* **1970**, *92*, 1551−1557.
(25) Bakac, A.; Brynildson, M. E.; Espenson, J. H. *Inorg. Chem.* **1986**, *25*, 4108−4114.
(26) Rangel, M.; Leite, A.; Gomes, J.; de Castro, B. *Organometallics* **2005**, *24*, 3500−3507.
(27) Rangel, M.; Arcos, T.; de Castro, B. *Organometallics* **1999**, *18*, 3451−3456.
(28) Arcos, T.; Decastro, B.; Ferreira, M. J.; Rangel, M.; Raynor, J. B. *J. Chem. Soc., Dalton Trans.* **1994**, 369−377.
(29) Decastro, B.; Pereira, J.; Rangel, M. *Organometallics* **1991**, *10*, 3848−3855.
(30) Decastro, B.; Rangel, M.; Raynor, J. B. *J. Chem. Soc., Dalton Trans.* **1990**, 3311−3318.
(31) Schrauzer, G. N.; Lee, L. P. *J. Am. Chem. Soc.* **1968**, *90*, 6541−6543.
(32) Wirt, M. D.; Bender, C. J.; Peisach, J. *Inorg. Chem.* **1995**, *34*, 1663−1667.
(33) Baumgarten, M.; Lubitz, W.; Winscom, C. J. *Chem. Phys. Lett.* **1987**, *133*, 102−108.
(34) Tyrlik, S.; Kwiecinski, M.; Rockenbauer, A.; Gyor, M. *J. Coord. Chem.* **1982**, *11*, 205−212.
(35) Rockenbauer, A.; Budozahonyi, E.; Simandi, L. I. *J. Chem. Soc., Dalton Trans.* **1975**, 1729−1737.
(36) Wasielewski, M. R. *J. Org. Chem.* **2006**, *71*, 5051−5066.
(37) Poluektov, O. G.; Utschig, L. M.; Schlesselman, S. L.; Lakshmi, K. V.; Brudvig, G. W.; Kothe, G.; Thurnauer, M. C. *J. Phys. Chem. B* **2002**, *106*, 8911−8916.
(38) Hyde, J. S.; Pasenkiewicz-Gierula, M.; Jesmanowicz, A.; Antholine, W. E. *Appl. Magn. Reson.* **1990**, *1*, 483−496.
(39) Stoll, S.; Schweiger, A. *J. Magn. Reson.* **2006**, *178*, 42−55.
(40) Lee, C. T.; Yang, W. T.; Parr, R. G. *Phys. Rev. B* **1988**, *37*, 785−789.
(41) Becke, A. D. *J. Chem. Phys.* **1993**, *98*, 5648−5652.
(42) Vosko, S. H.; Wilk, L.; Nusair, M. *Can. J. Phys.* **1980**, *58*, 1200−1211.
(43) Baker, J.; Wolinski, K.; Malagoli, M.; Kinghorn, D.; Wolinski, P.; Magyarfalvi, G.; Saebo, S.; Janowski, T.; Pulay, P. *J. Comput. Chem.* **2009**, *30*, 317−335.
(44) Klamt, A.; Schüürmann, G. *J. Chem. Soc., Perkin Trans. 2* **1993**, 799−805.
(45) Neese, F. *ORCA−An Ab Initio, DFT and Semiempirical SCF-MO Package - Version 2.8*; Lehrstuhl für Theoretische Chemie, Universität Bonn: Bonn, Germany, 2010.
(46) Schäfer, A.; Horn, H.; Ahlrichs, R. *J. Chem. Phys.* **1992**, *97*, 2571−2577.
(47) Weigend, F.; Ahlrichs, R. *Phys. Chem. Chem. Phys.* **2005**, *7*, 3297−3305.
(48) Wachters, A. J. H. *J. Chem. Phys.* **1970**, *52*, 1033−1036.
(49) Bauschlicher, C. W.; Langhoff, S. R.; Partridge, H.; Barnes, L. A. *J. Chem. Phys.* **1989**, *91*, 2399−2411.
(50) Bühl, M.; Kabrede, H. *J. Chem. Theory Comput.* **2006**, *2*, 1282−1290.
(51) Waller, M. P.; Bühl, M. *J. Comput. Chem.* **2007**, *28*, 1531−1537.
(52) Neese, F. *J. Chem. Phys.* **2001**, *115*, 11080−11096.
(53) Nishida, Y.; Kida, S. *Coord. Chem. Rev.* **1979**, *27*, 275−298.
(54) Stone, A. J. *Proc. R. Soc. A* **1963**, *271*, 424−424.
(55) Dunn, T. M. *Trans. Faraday Soc.* **1961**, *57*, 1441−1444.
(56) Malatesta, V.; McGarvey, B. R. *Can. J. Chem.* **1975**, *53*, 3791−3800.
(57) McGarvey, B. R. *Can. J. Chem.* **1975**, *53*, 2498−2511.
(58) Jones, R. D.; Summerville, D. A.; Basolo, F. *Chem. Rev.* **1979**, *79*, 139−179.
(59) Busch, D. H.; Alcock, N. W. *Chem. Rev.* **1994**, *94*, 585−623.
(60) Smith, T. D.; Pilbrow, J. R. *Coord. Chem. Rev.* **1981**, *39*, 295−383.
(61) Lubitz, W.; Winscom, C. J.; Diegruber, H.; Moseler, R. *Z. Naturforsch., A: Phys. Sci.* **1987**, *42*, 970−986.
(62) Jörin, E.; Schweiger, A.; Günthard, H. H. *Chem. Phys. Lett.* **1979**, *61*, 228−232.
(63) Hoffman, B. M.; Diemente, D. L.; Basolo, F. *J. Am. Chem. Soc.* **1970**, *92*, 61−65.
(64) Van Doorslaer, S.; Zingg, A.; Schweiger, A.; Diederich, F. *ChemPhysChem* **2002**, *3*, 659−667.
(65) Baumgarten, M.; Winscom, C. J.; Lubitz, W. *Appl. Magn. Reson.* **2001**, *20*, 35−70.
(66) Hohenester, E.; Kratky, C.; Krautler, B. *J. Am. Chem. Soc.* **1991**, *113*, 4523−4530.
(67) Van Doorslaer, S.; Schweiger, A.; Krautler, B. *J. Phys. Chem. B* **2001**, *105*, 7554−7563.
(68) Zbiri, M. *Inorg. Chim. Acta* **2006**, *359*, 3865−3870.
(69) Muckerman, J. T.; Fujita, E. *Chem. Commun.* **2011**, *47*, 12456−12458.
(70) Solis, B. H.; Hammes-Schiffer, S. *Inorg. Chem.* **2011**, *50*, 11252−11262.
(71) Siegbahn, P. E. M.; Blomberg, M. R. A. *Chem. Rev.* **2000**, *100*, 421−437.
(72) Orio, M.; Pantazis, D. A.; Neese, F. *Photosynth. Res.* **2009**, *102*, 443−453.
(73) Schoneboom, J. C.; Neese, F.; Thiel, W. *J. Am. Chem. Soc.* **2005**, *127*, 5840−5853.

(74) Noodleman, L.; Lovell, T.; Han, W. G.; Li, J.; Himo, F. *Chem. Rev.* **2004**, *104*, 459−508.
(75) Siegbahn, P. E. M.; Borowski, T. *Acc. Chem. Res.* **2006**, *39*, 729−738.
(76) Grabowski, S. J. *Hydrogen Bonding—New Insights*; Springer: Dordrecht, The Netherlands, 2006; Vol. 3.
(77) Jeffrey, G. A.; Saenger, W. *Hydrogen Bonding in Biological Structures*, Springer-Verlag: Berlin, 1991.
(78) Steiner, T. *Angew. Chem. Int. Ed.* **2002**, *41*, 48−76.
(79) Patchkovskii, S.; Ziegler, T. *J. Chem. Phys.* **1999**, *111*, 5730−5740.
(80) Munzarova, M.; Kaupp, M. *J. Phys. Chem. A* **1999**, *103*, 9966−9983.
(81) Munzarova, M. L.; Kubacek, P.; Kaupp, M. *J. Am. Chem. Soc.* **2000**, *122*, 11900−11913.
(82) Neese, F. *J. Phys. Chem. A* **2001**, *105*, 4290−4299.
(83) Tovrog, B. S.; Drago, R. S. *J. Am. Chem. Soc.* **1974**, *96*, 6765−6766.
(84) Tovrog, B. S.; Kitko, D. J.; Drago, R. S. *J. Am. Chem. Soc.* **1976**, *98*, 5144−5153.
(85) Utschig, L. M.; Silver, S. C.; Mulfort, K. L.; Tiede, D. M. *J. Am. Chem. Soc.* **2011**, *133*, 16334−16337.